JOURNAL OF MATERIALS SCIENCE 21 (1986) 2347–2355

Inelastic deformation of (Ti, V)C alloys

Part 1 *Hot-pressing kinetics*

VIVEK M. SURA*, D. L. KOHLSTEDT
Department of Materials Science and Engineering, Cornell University, Ithaca, New York 14853, USA

The densification behaviour of (Ti, V)C alloys was studied in order to prepare fully dense, single phase alloys. The hot-pressing experiments were conducted on two compositions, TiC and TiC–75% VC, at temperatures between 1300 and 1900° C and pressure up to 120 MPa. The effects of temperature and composition on final porosity, grain size and phases present were determined. The diffusion coefficients determined from densification data agree well with the grain-boundary diffusion coefficient of carbon. This observation, combined with microstructural evidence, indicates that the final stage of densification is controlled by grain-boundary diffusion of carbon and/or metal. The enhanced densification and grain growth in VC rich samples are attributed to the presence of second phase material along the grain boundaries. The rapid interdiffusion of titanium and vanadium in (Ti, V)C to form a single phase, raises the possibility of faster diffusion along the migrating boundaries in contrast to the stationary boundaries.

1. Introduction

The demand for structural materials for both low and high temperature applications is increasing rapidly. The cubic transition metal monocarbides of Groups IV and V possess a unique set of properties for such applications, including very high melting points, extremely high strength and excellent wear resistance. Of these carbides, TiC and VC have considerably lower densities than NbC, TaC, and HfC. Thus, they are potentially more useful because of their large strength to density ratio. However, these same properties impose significant manufacturing difficulties.

To produce high density carbides, a low melting binder phase such as nickel, cobalt or iron is often added. With a base-metal binder, dense material can be sintered at relatively low temperatures; however, the binder also limits the upper temperature at which the two phase cermet can be used. Alternatively, single phase carbide powders can be fabricated to full density in the absence of a liquid phase by hot-pressing [1–3].

Both titanium and vanadium monocarbides have the rock salt structure over a wide range of carbon to metal ratio with an appreciable vacancy concentration on the carbon sublattice [4]. Titanium carbide and vanadium carbide form a continuous solid solution series [5]. Consequently the mechanical properties of (Ti, V)C alloys not only depend on Me/C ratio (Me = metal), but also on Ti/V ratio. In this connection, the present work was undertaken to study the densification behaviour of these alloys in order to prepare fully dense, single phase alloys for subsequent mechanical testing experiments [6]. The hot-pressing experiments were conducted on two compositions, TiC and TiC–75 wt % VC, at temperatures between 1300 and 1900° C.

2. Experimental technique

2.1. Experimental apparatus

All of the hot-pressing experiments were conducted in a high temperature furnace mounted on a screw driven mechanical testing machine. The tungsten mesh element, which was resistively heated, was enclosed in a cylindrical heat shield assembly composed of concentric layers of molybdenum sheets. The furnace chamber was water cooled. The portions of the push rods which were inside the furnace, as well as the die cases, were fabricated from high strength graphite. One pushrod was attached to the cross-head of the testing machine, while the other was stationary and attached to the load cell. An automatic closed-loop control, utilizing tungsten–5% rhenium/tungsten–26% rhenium thermocouple, was used to maintain the temperature. All the experiments were conducted in an argon atmosphere.

2.2. Test materials

The starting materials employed were commercially available, near stoichiometric TiC and VC powders. The average particle size of TiC and VC powders were 4 and 3 μm, respectively. The particle size distributions are given in Table I. The carbon and oxygen levels were measured by decomposing the samples under oxidizing and reducing conditions, respectively, and analysing the evolved gases by infrared spectroscopy. The powder purity was determined by flame-emission spectroscopy. As indicated in Table II, oxygen was a primary contaminant in both powders. Some metal

*Present address: IBM East Fishkill, Hopewell Junction, New York 12533, USA.

0022–2461/86 $03.00 + .12

TABLE I Particle size distribution of starting powders.

Particle size (μm)	TiC	VC
	(percent of total)	
>8	1	3
4–8	44	15
2–4	37	52
1–2	14	24
<1	4	6

impurities (copper, iron, chromium and nickel) were detected, presumably arising from milling operations during the manufacturing of the powders. The carbon to metal ratio for the TiC powder was 0.94 with 0.6% unreacted carbon, while the same ratio for VC powder was 0.86, with 0.9% unreacted carbon.

2.3. Experimental procedure

Titanium carbide and vanadium carbide powders were subjected to a thorough dry mixing for a minimum of 6 h. The powder charges were placed in cylindrical graphite dies of 6.35 mm inner diameter and 25.4 mm length. Subsequently, these powders were cold pressed at a pressure of 70 MPa. The cold pressed samples were then uniaxially hot-pressed at the desired temperature. The heating and cooling rate of the furnace was ~ 25 to 30° C min^{-1}.

It was a standard practice to apply 25 to 30 MPa throughout the heating period. After reaching the desired temperature, the pressure was applied by moving the cross-head downward at a constant compression rate of 0.005 cm min^{-1}. The maximum pressure applied was limited by the compressive strength (160 MPa) of the die material. It is important to note that because of the way the pressure was applied, the densification rate was a controlled variable, while the stress was a dependent variable. Therefore, the data from a hot-pressing run were recorded as load against time on a magnetic tape for later analysis on a computer.

Specimens for optical microscopy were diamond cut from the hot-pressed samples and then polished by normal metallographic techniques. An etchant of 1 : 1 : 3 solution of nitric, hydrofluoric, and lactic acids was used to reveal the microstructure of TiC samples, while an etchant made of 15 g $K_3Fe(CN)_6$, 2 g NaOH, and 100 ml water was used for TiC–75% VC [7]. Grain sizes were determined on photo-micrographs using the linear intercept technique with a correction factor of 1.5. Density of the samples at the end of a hot-pressing run was measured by the water immersion technique.

X-ray diffraction was used to determine the major crystalline phases present. Portions of mechanically thinned samples were ion thinned to produce specimens for transmission electron microscopy (TEM). These foils were examined on a Siemens 102 transmission electron microscope and a JEOL 200CX scanning transmission electron microscope (STEM).

TABLE II Chemical analysis of starting powders.

Sample	Element	Concentration (wt %)
TiC	C	18.8
	O	0.49
	Co	0.03–0.1
	Fe, Ni	0.01–0.03
VC	C	16.7
	O	3.49
	Cr, Fe	0.1–0.3
	Ni	0.03–0.1
	Co	0.01–0.03

2.4. Data processing

The load–time data were analysed to obtain stress, density and densification rate as a function of time. The height of the sample, $L(t)$, at a given time t during densification can be calculated from the relation

$$L(t) = L_0 - \dot{X}t \quad (1)$$

where L_0 is the height of the sample at the start of hot-pressing and $\dot{X}$ the cross-head velocity. The density, $\varrho(t)$, of the sample at a given time during densification is given by

$$\varrho(t) = (M/A)\,(1/L(t)) \quad (2)$$

where M is the mass of the sample and A the cross-sectional area. Both M and A are constant in the hot-pressing die. Thus, from the calculation of the height of the sample, the densities at various stages of a hot-pressing run were determined.

The densification rate during hot-pressing was calculated by combining Equation 1 with Equation 2 and differentiating

$$1/\varrho\,\mathrm{d}\varrho/\mathrm{d}t = -\dot{L}(t)/L(t) = \dot{X}/L(t) \quad (3)$$

As mentioned earlier, the cross-head velocity, $\dot{X} = 0.005$ cm min^{-1}, was used for applying load. Typically, the height of a sample varied from ~ 1.8 cm at the start of the hot-pressing to ~ 1.3 cm at the end of the hot-pressing. According to Equation 3, the resulting densification rate would vary between $\sim 4.6 \times 10^{-5}$ and $\sim 6.4 \times 10^{-5}$ sec^{-1}.

The effective stress on a porous sample is greater than the applied stress and was taken to be [8]

$$\sigma_{\mathrm{eff}} = \sigma_{\mathrm{app}}[\varrho_{\mathrm{th}}/\varrho(t)] \quad (4)$$

where σ_{eff} is the effective stress, σ_{app} the applied stress and ϱ_{th} the theoretical density. The driving force for hot-pressing results from the applied stress corrected for porosity, σ_{eff}, and the surface energy of the pore. Any sample will, of course, exhibit a range of pore radii. In addition, the average pore size is a function of time and density. If the pore radius, r, is approximated by [8]

$$r = (1 - \varrho/\varrho_{\mathrm{th}})^{1/3}(G/2) \quad (5)$$

where G is the grain size, and if a value of 1.19 J m^{-2} is used for the surface energy [9], the stress resulting from the surface tension at 90% of theoretical density would be $2\gamma/r \sim 1$ MPa for a specimen with an average grain size 10 μm. This value is approximately two orders of magnitude smaller than the effective stress, $\sigma_{\mathrm{eff}} \sim 35$ to 120 MPa. Therefore, to simplify the analyses, the driving force due to surface energy is neglected.

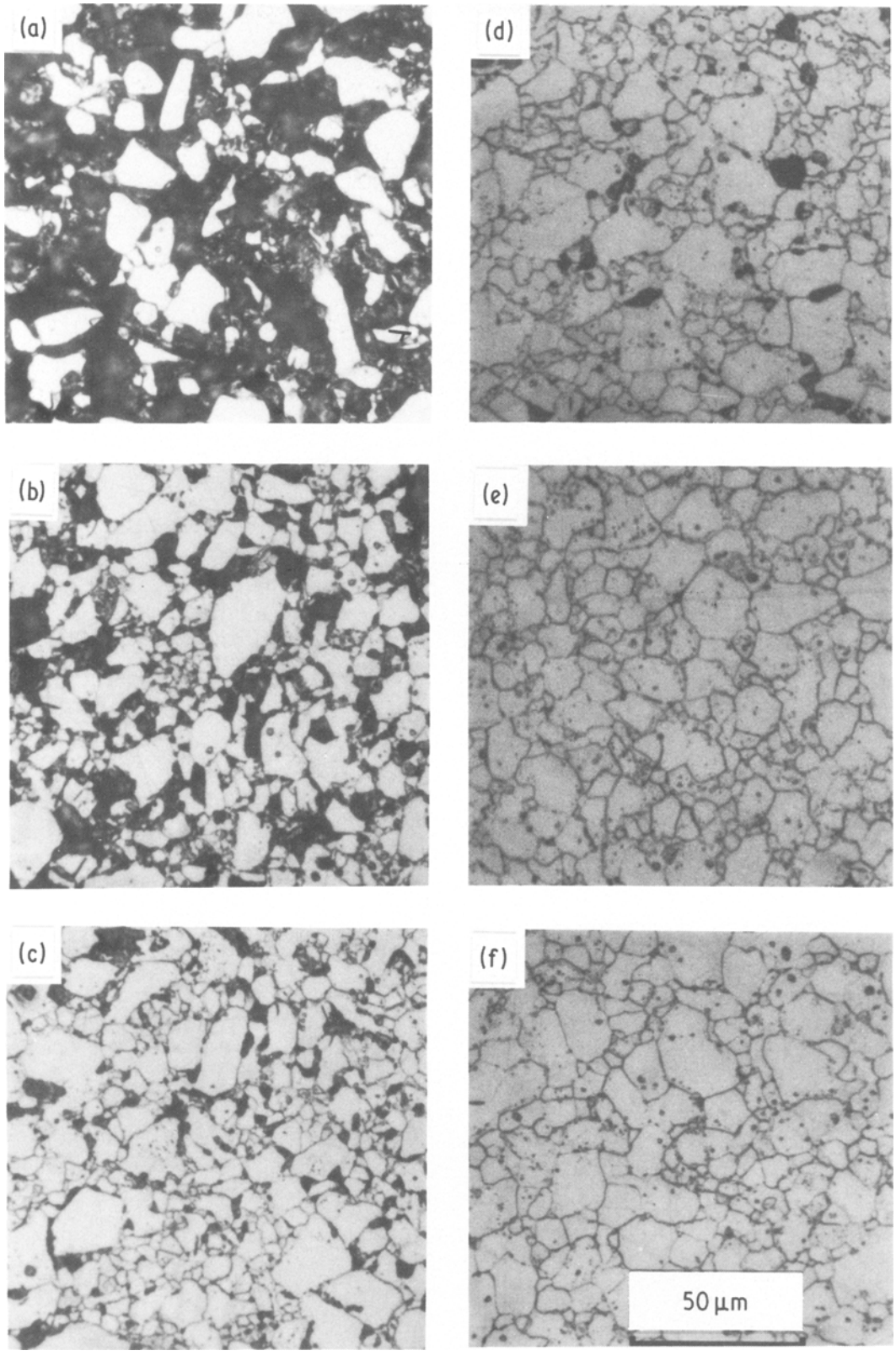

Figure 1 Optical micrographs of as-hot-pressed TiC at (a) 1400, (b) 1500, (c) 1600, (d) 1700, (e) 1800, (f) 1900° C.

3. Results

X-ray diffraction data demonstrate that all the hot-pressed samples are single phase. The composition of these samples is either TiC or TiC ~ 75% VC, both in the single phase region of TiC–VC solid solution. Optical micrographs of TiC and TiC–75% VC samples hot-pressed at different temperatures are shown in Figs 1 and 2. Pores are distributed mainly along the grain boundaries, and there is no evidence of discontinuous grain growth.

The density of TiC samples increased with increasing hot-pressing temperature. The average grain size for these samples ranged from 6 μm at 1400° C to 10 μm at 1900° C. The TiC–75% VC samples appeared to have high densities and uniform grain sizes over the complete range of hot-pressing temperature. The grain size increased from 5 μm at 1300° C to 16 μm at 1800° C. TEM examinations supported these results, and also revealed only a sparse distribution of dislocations. The dislocations were primarily observed

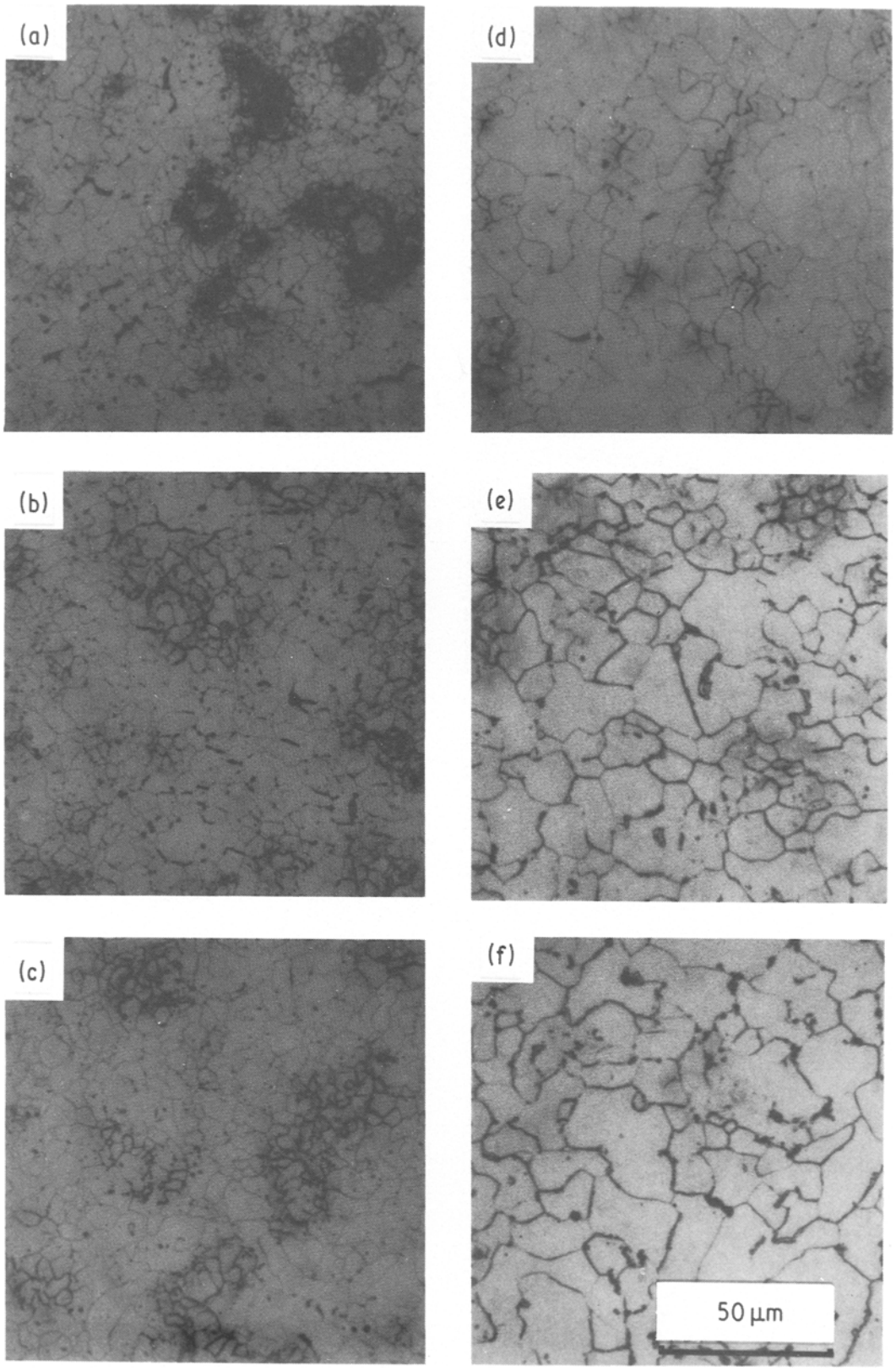

Figure 2 Optical micrographs of as-hot-pressed TiC–75% VC at (a) 1300, (b) 1400, (c) 1500, (d) 1600, (e) 1700, (f) 1800° C.

along the grain boundaries and along the second phase particles, apparently resulting from the stress concentration at these sites.

TEM observations also revealed the accumulation of impurities into second phase particles along the grain boundaries and in some of the triple junctions, Fig. 3. Energy-dispersive spectroscopy data obtained with the STEM indicate that the particles mainly contain cobalt, iron and nickel. The distribution of these elements was nonuniform in the second phase particles, therefore a single grain boundary composition could not be identified. A typical spectrum is shown in Fig. 4. The titanium and vanadium peaks come from the surrounding matrix, and the copper peak from the copper support washer.

The relative densities of the cold compacts ranged from 64 to 66% for TiC and from 56 to 58% for TiC–75% VC. However, the relative density at the start of

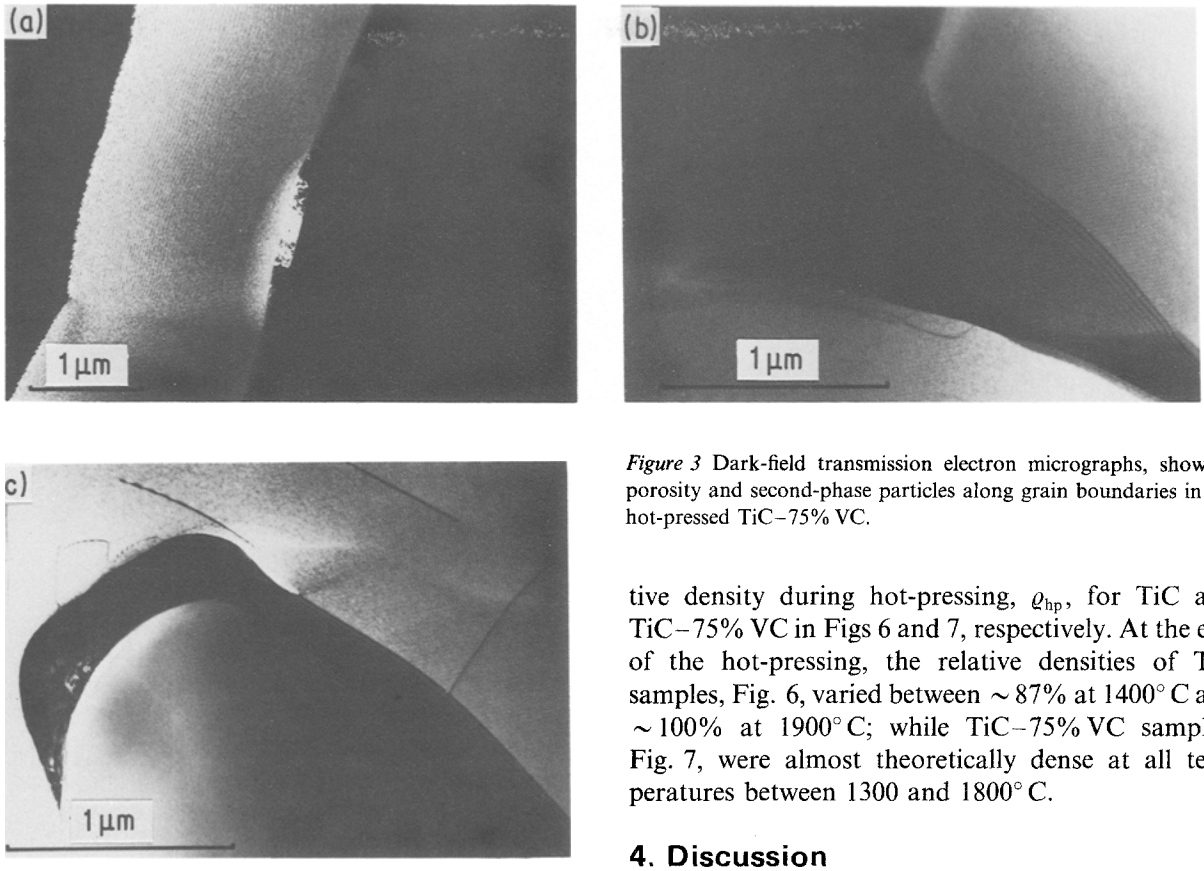

Figure 3 Dark-field transmission electron micrographs, showing porosity and second-phase particles along grain boundaries in as-hot-pressed TiC–75% VC.

the hot-pressing, ϱ_{sin}, which represents the densification during heating period, was substantially higher for TiC–75% VC samples than for the TiC samples at a given temperature. This effect is shown in Fig. 5, in which ϱ_{sin} is plotted as a function of temperature for both compositions. It can be seen in Fig. 5 that ϱ_{sin} varies linearly with temperature from ~77% at 1400° C to ~95% at 1900° C for TiC; while for TiC–75% VC samples, it increases from ~82% at 1300° C to ~96% ⩾1500° C. To describe the hot-pressing behaviour, effective stress is plotted against relative density during hot-pressing, ϱ_{hp}, for TiC and TiC–75% VC in Figs 6 and 7, respectively. At the end of the hot-pressing, the relative densities of TiC samples, Fig. 6, varied between ~87% at 1400° C and ~100% at 1900° C; while TiC–75% VC samples, Fig. 7, were almost theoretically dense at all temperatures between 1300 and 1800° C.

4. Discussion

Final stage densification during the hot-pressing is most important for achieving fully dense samples. In this stage, pores are closed and roughly spherical in shape. Densification during the final stage is attributable to either some form of diffusional viscous flow or to dislocation mechanisms under the combined driving force of surface tension and external pressure. If densification is controlled by lattice diffusion (Nabarro–Herring creep) [10, 11], the densification rate is given by

$$1/\varrho\, \mathrm{d}\varrho/\mathrm{d}t = (40D_L\Omega/3G^2kT)(\sigma_{eff} + 2\gamma/r) \quad (6)$$

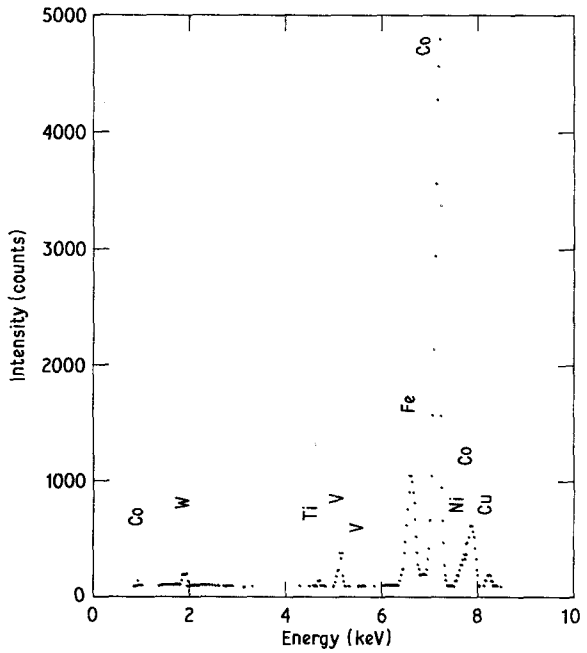

Figure 4 Energy dispersive spectrum from the second phase particle in the grain boundary of as-hot-pressed TiC–75% VC.

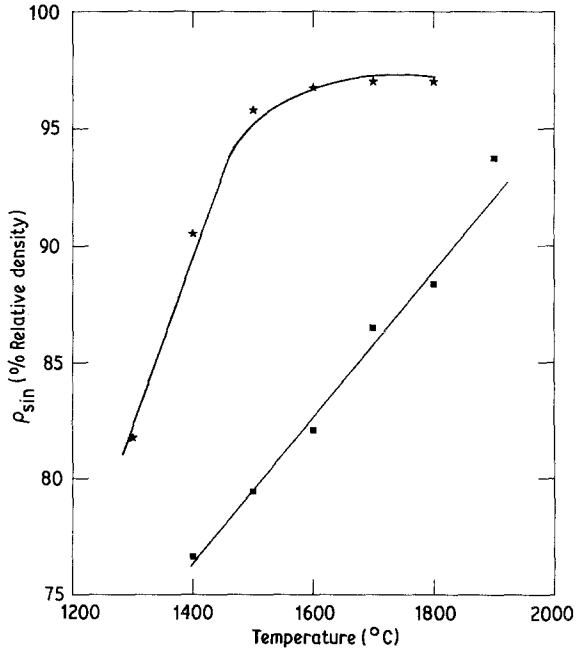

Figure 5 ϱ_{sin} against temperature for (■) TiC and (★) TiC–75% VC.

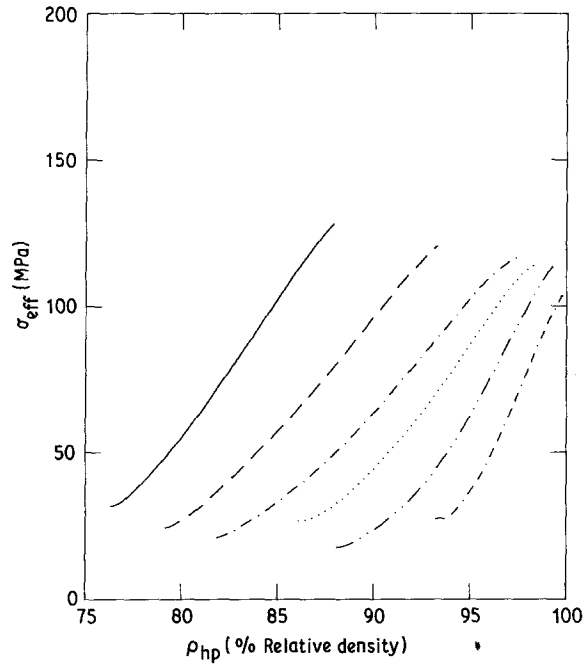

Figure 6 Effective stress against relative density during hot-pressing of TiC at (——) 1400, (– –) 1500, (– · –) 1600, (·····) 1700, (– ·· –) 1800 and (– – · –) 1900° C.

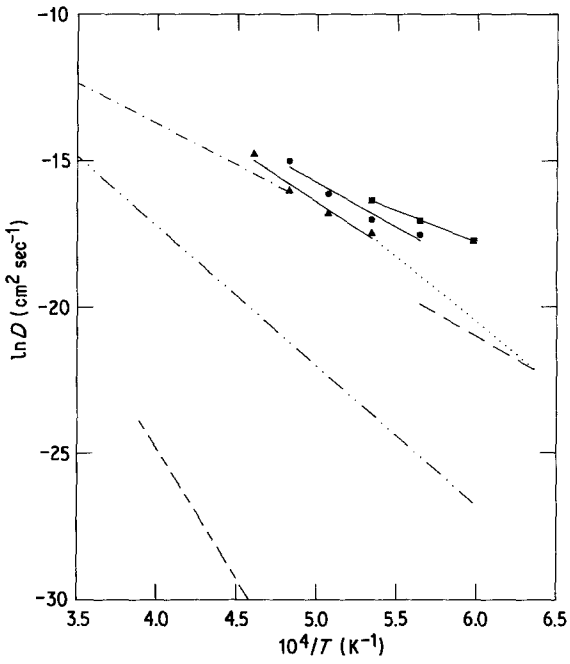

Figure 8 Arrhenius plot of diffusion coefficients of carbon and titanium in TiC. (– –) Vansant and Phelps [18], (– · –) Adelsberg and Cadoff [17], (·····) Quinn and Kohlstedt [19], (– ·· –) Sarian for carbon [15], (– · –) Sarian for titanium [16], (——) present study. ϱ = (■) 85, (●) 90 and (▲) 95%.

where D_L is the lattice diffusion coefficient, Ω an atomic volume, G the grain size, and k Boltzmann's constant. If the fastest diffusional path is along the grain boundaries, then the rate of densification is controlled by grain-boundary diffusion (Coble creep) [12], and the densification rate may be expressed as

$$1/\varrho\, d\varrho/dt = (47.5 D_b \Omega\delta/G^3 kT)(\sigma_{eff} + 2\gamma/r) \quad (7)$$

where δ is the grain boundary width and D_b the grain boundary diffusion coefficient. At high stresses, densification is accomplished by climb and glide of dislocations, and the observed densification rate follows the semi-empirical relation [13]

$$1/\varrho\, d\varrho/dt = (AD_L b\mu/kT)[(\sigma_{eff} + 2\gamma/r)/\mu]^n \quad (8)$$

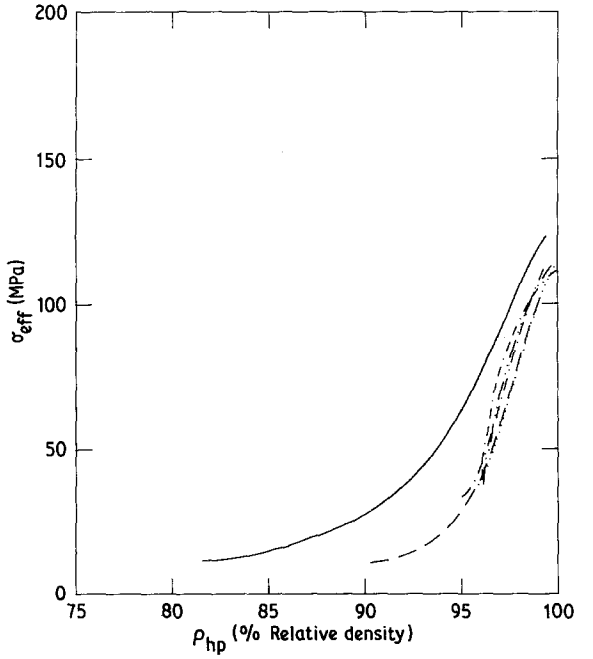

Figure 7 Effective stress against relative density during hot-pressing of TiC–75% VC at (——) 1300, (– –) 1400, (– · –) 1500, (·····) 1600, (– ·· –) 1700 and (– – · –) 1800° C.

where A is an empirical constant, b the Burgers vector, μ the shear modulus and n the stress exponent.

The absence of extensive dislocation structure in the hot-pressed samples, Fig. 3, suggests that densification is controlled by diffusive mechanisms rather than by dislocation climb and glide. Thus, the lattice diffusion coefficients were calculated using Equation 6. The resulting values for D_L were considerably greater than the lattice self-diffusion coefficients in these carbides, suggesting that densification must be controlled by the diffusion along the grain boundaries. Chermant *et al.* [9] performed sintering experiments at 1900 to 2400° C, on TiC with grain size 0.1 and 10 μm. They also observed that the final stage of sintering is controlled by grain-boundary diffusion.

Assuming that the densification is controlled by the diffusion along the grain boundaries, the hot-pressing data were analysed in terms of Equation 7. Neglecting the surface energy term, Equation 7 can be rewritten as

$$D_b = [(1/\varrho\, d\varrho/dt)G^3 kT/47.5\Omega\delta\sigma_{eff}] \quad (9)$$

Thus, using Equation 9, the diffusion coefficients for TiC at various temperatures were determined from Fig. 6, at ϱ = 85, 90 and 95%. The densification rate was calculated from Equation 3, and the grain size at the end of the hot-pressing was substituted for G. A value of $20.2816 \times 10^{-30}\,m^3$ was used for atomic volume, Ω [4], and 1×10^{-9} m for grain-boundary width, δ [14]. The calculated values for the boundary diffusivity for TiC are shown as an Arrhenius plot in Fig. 8.

The results of the present study are compared with those reported in the literature for carbon and titanium diffusion in titanium carbide. Sarian determined the diffusion coefficients for carbon [15] and metal [16]

self-diffusion in TiC_x single crystals by tracer techniques. These values represent the lattice diffusion of carbon and titanium in the carbide. The data of Adelsberg and Cadoff [17] and Vansant and Phelps [18] represent short circuit diffusion of carbon along the grain boundaries, as these diffusivities were determined by carburization of titanium metal. The work by Quinn and Kohlstedt on the TiC–Ti diffusion couple yielded similar results [19]. The diffusion coefficients obtained in this study lie considerably above the tracer diffusion coefficients and are in good agreement with those obtained for boundary diffusion. Therefore, it can be concluded that the final stage densification is controlled by grain-boundary diffusion of carbon and/or titanium in TiC.

As described earlier, TiC–75% VC samples were ~95% dense at the start of hot-pressing. Therefore, the hot-pressing data of TiC–75% VC (Fig. 7) could not be analysed using Equation 9. The better densification characteristics of TiC–75% VC cannot be attributed to the differences in melting point or grain sizes of two compositions. The melting point of stoichiometric TiC is ~2776° C, while that of TiC–75% VC is ~2600° C [5]. The average starting particle size of VC powder was 3 μm compared to 4 μm for TiC. The self diffusion coefficients of carbon and vanadium in VC [20, 21] are comparable to those of carbon and titanium in TiC [15, 16]; therefore the variation in the lattice diffusion coefficients as a reason of enhanced densification also can be ruled out.

The role of powder impurities in determining densification kinetics has to be examined. Leipold and Becher [22] found that densification and grain growth in tantalum carbide during hot-pressing was extremely sensitive to minor variations in grain-boundary chemistry. They observed enhanced densification and grain growth with increased oxygen content due to formation of Ta_2O_5, which accumulated along the grain boundaries. Both titanium and vanadium form a series of oxides [23, 24]; particularly, the V_2O_3–V_2O_5 system results in a liquid phase due to the eutectic reaction at ~660° C. Unfortunately, the distribution of oxygen in TiC–75% VC could not be examined in the electron microprobe studies, as L_β line for vanadium coincides with K_α line for oxygen; however, its effect on densification cannot be ruled out.

The presence of second phase material rich in cobalt, nickel, iron and chromium along the grain boundaries in the hot-pressed TiC has been observed before [2, 3, 25]. According to Katz *et al.* [25], the impurities in the grain boundaries form low-melting phases by complex eutectic reactions. The low-melting point phases soften and/or melt between 600 and 1200° C, resulting in a liquid phase along the grain. As Co–C and Fe–C systems form eutectic boundaries at 1309 and 1147° C, respectively, the presence of free carbon in the starting powder also causes a significant drop in the temperature at which softening begins.

The effect of this "localized" liquid phase along grain boundaries on densification and grain growth of carbides has not been studied before. However, microstructural development during the liquid phase sintering of cemented carbides of TiC, HfC, VC, NbC and TaC with 5 to 30% cobalt binder phase has been studied by Warren and Waldron [26], giving considerable relevant information on wetting characteristics. According to these authors, for a given volume fraction of cobalt, VC shows lower carbide contiguity, lower dihedral angle and lower angle of contact than does TiC, suggesting that wetting of grain boundaries is more complete in the VC–Co system than in the TiC–Co system. From the recent findings by Warren [27], a similar conclusion can be drawn for other metals as iron and nickel in VC and TiC.

Thus, the enhanced densification and grain growth behaviour of TiC–75% VC might be due to the liquid phase which forms along the grain boundaries from the metal impurities, plus free carbon and oxygen. The concentration of impurities is higher in the VC powder than in the TiC powder. The higher fraction of melt and the better wetting characteristics of VC result in higher grain boundary mobility and, in turn, better densification of TiC–75% VC in comparison to TiC. Optical micrographs of TiC, TiC–75% VC and VC, hot-pressed at 1750° C for 1 h (Fig. 9) show the effect of increasing the VC and impurity content on the grain boundary mobility. The grain boundary mobility is so high in VC that the boundaries detach themselves from the pores during the early stages of densification. Lattice diffusion is essential to eliminate this entrapped porosity. As the densification is controlled by grain-boundary diffusion in these carbides, the pores which are left behind by the migrating boundaries can be seen in Fig. 9c.

X-ray diffraction as well as electron microprobe studies revealed the formation of a single phase TiC–75% VC solid solution after hot-pressing for 45 to 60 min at 1300 to 1800° C. To form a single phase solid solution, interdiffusion of titanium and vanadium in the carbide matrix is essential. The interdiffusion coefficient of titanium and vanadium in (Ti, V)C can be expressed as [28]

$$\tilde{D}(N_V) = [N_V D_{Ti}(N_V) + N_{Ti} D_V(N_V)]\, \partial \ln a_V / \partial \ln N_V \quad (10)$$

where $\tilde{D}(N_V)$ is the inter-diffusion coefficient for titanium and vanadium in (Ti, V)C at a given composition, N_V the mole fraction of vanadium, N_{Ti} the mole fraction of titanium, $D_{Ti}(N_V)$ the self diffusivity of titanium in (Ti, V)C at a given composition, $D_V(N_V)$ the self diffusivity of vanadium in (Ti, V)C at a given composition and $\partial \ln a_V / \delta \ln N_V$ the thermodynamic factor. From $\tilde{D}$, the time required for the interdiffusion of titanium and vanadium in (Ti, V)C can be estimated and compared with experimental findings. However, no data are available either for D_{Ti} and D_V in (Ti, V)C or for the thermodynamic factor. Thus, $\tilde{D}$ could not be estimated.

To investigate the rapid homogenization observed during hot-pressing, a diffusion couple of TiC and VC was prepared by annealing single crystals at 1500° C for 3 h. The concentration profile was measured with an electron microprobe. The chemical diffusivities were determined using the Boltzmann–Matano method [29]. $\tilde{D}$ for TiC–75% VC at 1500° C was found to be $\sim 3.3 \times 10^{-13}\,cm^2\,sec^{-1}$ which is faster

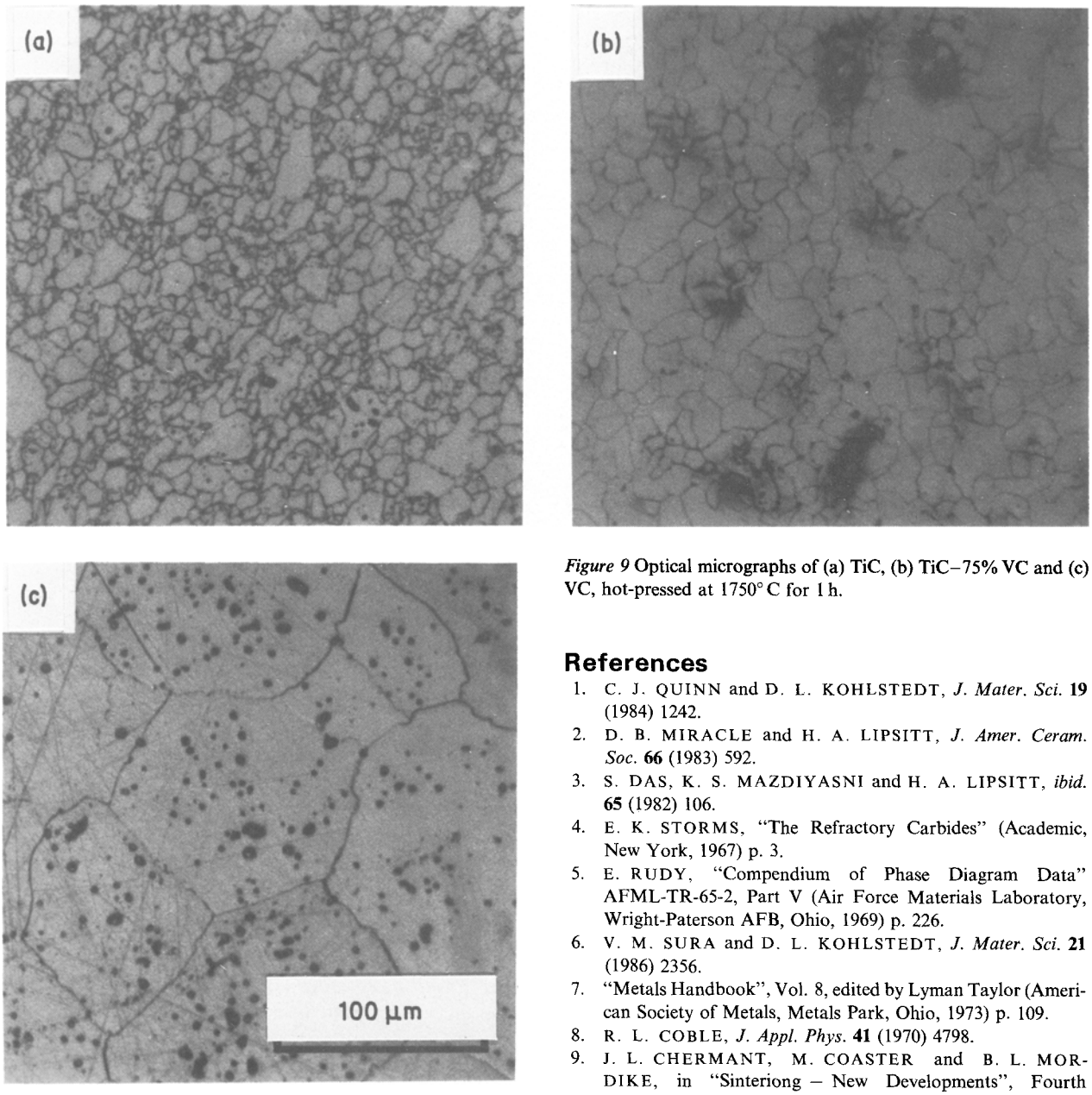

Figure 9 Optical micrographs of (a) TiC, (b) TiC–75% VC and (c) VC, hot-pressed at 1750° C for 1 h.

than either tracer diffusivity of vanadium in VC ($2.5 \times 10^{-14}\,cm^2\,sec^{-1}$) [21] or tracer diffusivity of titanium in TiC ($7.5 \times 10^{-18}\,cm^2\,sec^{-1}$) [15]. Using this value of $\tilde{D}$ at 1500° C, the time required for homogenization of titanium and vanadium by interdiffusion over a distance of 3 to 5 μm (approximately half the grain size) would have been 19 and 53 h, respectively. In the present study, anomalously short times, ~45 to 60 min, were observed to form a single phase (Ti, V)C solid solution. As discussed earlier, the grain boundaries in (Ti, V)C migrate considerably during the hot-pressing and grain growth. This raises the possibility that diffusional mass transport by migrating grain boundaries leads to rapid homogenization [30].

Acknowledgements

This research was supported by the Department of Energy through grant number DE-AC02-77ER04441. The electron microscopy was carried out in the Central Facility for Electron Microscopy which is part of the Materials Science Center at Cornell University.

References

1. C. J. QUINN and D. L. KOHLSTEDT, *J. Mater. Sci.* **19** (1984) 1242.
2. D. B. MIRACLE and H. A. LIPSITT, *J. Amer. Ceram. Soc.* **66** (1983) 592.
3. S. DAS, K. S. MAZDIYASNI and H. A. LIPSITT, *ibid.* **65** (1982) 106.
4. E. K. STORMS, "The Refractory Carbides" (Academic, New York, 1967) p. 3.
5. E. RUDY, "Compendium of Phase Diagram Data" AFML-TR-65-2, Part V (Air Force Materials Laboratory, Wright-Paterson AFB, Ohio, 1969) p. 226.
6. V. M. SURA and D. L. KOHLSTEDT, *J. Mater. Sci.* **21** (1986) 2356.
7. "Metals Handbook", Vol. 8, edited by Lyman Taylor (American Society of Metals, Metals Park, Ohio, 1973) p. 109.
8. R. L. COBLE, *J. Appl. Phys.* **41** (1970) 4798.
9. J. L. CHERMANT, M. COASTER and B. L. MORDIKE, in "Sinteriong – New Developments", Fourth International Round Table Conference on Sintering, Dubrovnik, September 1977 (Elsevier, New York, 1979) p. 319.
10. F. R. N. NABARRO, Bristol Conference on Strength of Solids, Bristol, England, April 1948 (The Physical Society, London, 1948) p. 75.
11. C. HERRING, *J. Appl. Phys.* **21** (1950) 437.
12. R. L. COBLE, *ibid.* **34** (1963) 1679.
13. M. R. NOTIS, R. H. SMOAK and V. KRISHNAMACHARI, in "Sintering and Catalysis", Proceedings of the Fourth International Conference on Sintering and Related Phenomena, edited by G. C. Kuczynski (Plenum, New York, 1975) p. 493.
14. N. L. PETERSON, *Int. Met. Rev.* **28** (1983) 65.
15. S. SARIAN, *J. Appl. Phys.* **39** (1968) 3305.
16. *Idem, ibid.* **40** (1969) 3575.
17. L. M. ADELSBERG and L. H. CADOFF, *Trans. AIME* **239** (1967) 933.
18. C. A. VANSANT and W. C. PHELPS, *Trans. ASM* **59** (1966) 105.
19. C. J. QUINN and D. L. KOHLSTEDT, *J. Amer. Ceram. Soc.* **67** (1984) 305.
20. S. SARIAN, *J. Phys. Chem. Solids* **33** (1972) 1637.
21. G. L. DEPOORTER and G. L. WALLACE, in "Advances in High Temperature Chemistry" Vol. 4, edited by Leroy Eyring (Academic, New York, 1970) p. 107.
22. M. H. LEIPOLD and P. F. BECHER, *Amer. Ceram. Soc. Bull.* **49** (1970) 647.
23. E. M. LEVIN, C. R. ROBBINS and H. F. MuMURDIE, in "Phase Diagrams for Ceramists", (American

Ceramic Society, Columbus, Ohio, 1964) p. 41.
24. E. M. LEVIN and H. F. MuMURDIE, in "Phase Diagrams for Ceramists, 1975 Supplement" (American Ceramic Society, Columbus, Ohio, 1975) p. 16.
25. A. P. KATZ, H. A. LIPSITT, T. MAH and M. G. MENDIRATTA, *J. Mater. Sci.* **18** (1983) 1983.
26. R. WARREN and M. B. WALDRON, *Powder Metall.* **15** (1972) 166.
27. R. WARREN, *J. Mater. Sci.* **15** (1980) 2489.
28. H. SCHMALZRIED, "Solid State Reactions" (Verlag Chemie, Weinheim, 1981) p. 131.
29. P. G. SHEWMAN, "Diffusion in Solids" (McGraw-Hill, New York, 1963) p. 29.
30. J. W. CAHN and R. W. BALLUFFI, *Scr. Met.* **13** (1979) 499.

Received 16 July
and accepted 13 September 1985